Journal of Applied Spectroscopy, Vol. 90, No. 2, May, 2023 (Russian Original Vol. 90, No. 2, March–April, 2023)

SYNTHESIS OF PRECURSORS FOR THE PRODUCTION OF NANOCERAMICS OF THE $CuAlO_2$ TYPE UNDER THE INFLUENCE OF DOUBLE LASER PULSES ON AD1 AND M2 ALLOYS IN AIR

E. S. Voropai,[a] N. A. Alekseenko,[b] M. N. Kovalenko,[a] L. V. Markova,[b] and A. P. Zazhogin[a,*]

UDC 533.9.082.5;621.373.826;621.793.79

The effect of the energy, the interval between the pulses, and the number of double laser pulses on the formation of the component and charge composition of laser plasma by laser spark spectrometry (LSS-1 spectrometer) was studied. The processes leading to the formation of mixed nanopowders of copper and aluminum oxides, precursors for the production of nanoceramics and films of $CuAlO_2$ copper aluminates by the action of double laser pulses on a hybrid target consisting of cemented aluminum and copper plates, from AD1 and M2 alloys were investigated. It was shown that precursors for the manufacture of nanoceramics and nanofilms of $CuAlO_2$ copper aluminates can be obtained by the successive action of a series of double laser pulses with energy of 53 mJ and an interval of 10 μs on a hybrid target. A closed glass weighing bottle containing the target was used for the products formed during interaction of the aluminum and copper ions with atmospheric oxygen. The size of the initial particles, determined by means of a high-resolution electron microscope, amounted to 30–45 nm. The particles were assembled into agglomerates and had a crystalline structure and spherical form. On account of the purely diffusion transfer mechanism of the fractals the size and amount of the fractal aggregates settling on the support situated at the bottom of the cuvette were several times greater than the amount of the products that settle on the side support. The main contribution to change in the intensity of the spectral lines for the Al and Cu atoms and ions and the AlO molecular bands comes from interaction of the second pulse with the condensation products formed in the channel after the action of the first pulse. With increase in the number of long-lived fractal aggregates in the air the intensity of molecular bands and lines decreases by ~1.5 times for Al III and by ~2 times for copper, which is due to active interaction of the long-lived large fractals that accumulate in the air with the incident radiation.

***Keywords**: Al_2O_3, AlO, CuO, Cu_2O, $CuAlO_2$, pulsed laser sputtering, laser plasma, laser spark spectrometry, nanoceramics.*

Introduction. Nanopowder technologies are currently some of the most widespread areas of development in nanotechnology. The nanopowders (NR) obtained by their use have found use in electronics, medicine, biology, chemical catalysis, and other regions of science and technology. For this reason the development of methods for the synthesis of nanoparticles (NP) with specific properties, the most important of which include the size, shape, chemical composition, structure, and degree of agglomeration of the NPs, is an important practical task [1–3].

The most universal methods for the production of NRs with minimal contamination and maximum practicability for the raw material used for the targets (coarse powders and their mixtures, metals, and alloys, mixtures of metals and nonmetals) involve evaporation by laser radiation and an electron beam and magnetron sputtering [4–7]. Most of the methods and particularly magnetron sputtering and electron beam evaporation require a rigorous high vacuum environment and a complex working process.

The advantage of laser radiation in the evaporation of most materials is the small depth of penetration of the beam into the material, which makes it possible to evaporate the target with relatively small energy consumption. Both continuous

*To whom correspondence should be addressed.

[a]Belarusian State University, Minsk, Belarus; email: zajogin_an@mail.ru; [b]Academician O. V. Roman Institute of Powder Metallurgy, Minsk, Belarus; email: alekseenkon@rambler.ru. Translated from Zhurnal Prikladnoi Spektroskopii, Vol. 90, No. 2, pp. 275–286, March–April, 2023. Original article submitted February 13, 2023; https://doi.org/10.47612/0514-7506-2023-90-2-275-286.

[5] and pulsed lasers with different pulse durations [6, 7] are used for evaporation of the targets. By the laser-chemical method it is possible to solve the task of creating and using the chemically active plasma produced as a result of the action of laser radiation on a gaseous medium.

A large role in the development of laser technologies has been played by the scientific school of Belarusian physicists under the leadership of academician of the Academy of Sciences of BSSR B. I. Stepanov, beginning with published papers on the theory of laser generation [8, 9].

Of particular interest in recent times are the thermoelectric characteristics of the semiconducting compound copper aluminate ($CuAlO_2$), which belongs to the group of transparent conducting oxides with hole-type electric conductivity (*p*-TCO) [10–14], with crystal structures of the delafossite type, which have the chemical formula AIBIIIO$_2$ where A I represents monovalent cations (Cu^+, Ag^+, Pd^+, etc.) and B III represents trivalent cations (Al^{+3}, Ga^{+3}, Cr^{+3}, etc.) [15]. A special feature of the delafossite type of structure is the presence of layers of Cu^{1+} (the *ab* plane), which alternate with layers of MO_6 octahedra formed by cations of M and the oxygen O and distributed along the edges. The octahedra are oriented along the *c* axis of the crystal structure. Another feature of the structure is the fact that each copper ion Cu^{1+} is in dual coordination with the oxygen, forming a "dumbbell-like" O–Cu–O structure that is connected to the MO_6 octahedron [16]. The layer structure reduces the Cu–Cu interaction and leads to an appreciable increase of band gap (E_g = 3.5–3.7 eV) compared with the oxide of monovalent copper Cu_2O, which also belongs to *p*-type semiconductors but is an isotropic compound with E_g = 2.1 eV. The main problem for practical applications of the $CuAlO_2$ semiconductor compound is its comparatively low thermal efficiency.

A significant shortcoming that restricts the application of single-pulse laser activity for the production of quality nanopowders at moderate power densities is the bulk evaporation mechanism, which can be the source of condensed matter and droplets in the evaporation products [17]. Its low efficiency is also a disadvantage. By using the schemes and methods of double-pulse laser action at different angles of incidence on the target and the plasma in air it is possible to carry out highly sensitive spectral analysis, to control the concentration of the excited and charged particles in plasma, and to control the composition of nanopowder precursors for the manufacture of nanoceramics simultaneously.

The aim of the present work was to determine the conditions for the production of nanopowders of Al, Cu, and Al_2O_3 oxides by ablation with a series of double laser pulses in air for use in technologies for the production of $CuAlO_2$ nanoceramics.

Experimental. An LSS-1 laser multichannel atomic emission spectrometer (SP LOTIS, TII, Belarus) was used. As source for ablation and excitation of the surface plasma the spectrometer included a two-pulse neodymium laser (model LS2131 DM) operating at a pulse repetition rate of up to 10 Hz at a wavelength of 1064 nm. The laser has a wide range of possibilities for adjusting both the pulse energy (up to 80 mJ) and the time shift between double radiation pulses (0–100 μs in steps of 1 μs). The pulse duration was ~15 ns. The laser radiation was focused onto the sample using an achromatic condenser with a focal length of 104 mm. The size of the focused spot was ~50 μm. A hybrid target consisting of plates of AD1 and M2 alloys glued together and placed in a closed rectangular glass cell 40 × 20 × 30 mm in size was used to obtain the nanopowder. A MIRA3 high-resolution scanning electron microscope (SEM) with an EDX X-Max x-ray spectral microanalyzer was used to analyze the products deposited on the surface of silicon plates placed outside the laser flame propagation zone (at the bottom and on one of the sides of the cuvette).

Analysis and targeted change of the component, charge, and energy distributions of the composition of the laser are possible on the basis of the effect of additional laser radiation on the primary plasma. The temperature of the laser plasma, in tens of thousands of degrees, determines the presence of ions, electrons, radicals, and neutral particles in the excited state. The presence of such particles leads to high interaction rates and fast (10^{-3}–10^{-8} s) reactions. The high temperature ensures transition of almost all the starting substances into the gas state with their subsequent interaction and condensation of the products. The emission spectrum of the plasma contains the lines of Al^+, Al^{2+}, Cu^{+1}, N^+, and O^+ ions, Al and Cu atoms, AlO and AlN molecules, and the gaseous medium.

The laser gas-phase production of the powders can be divided into two stages: evaporation of the target under the influence of the laser radiation and creation of a laser plasma containing the vapors of the metals as a source of the material being synthesized; synthesis of an ultradispersed powder from the vapor phase and the activated gas. The metal vapors form compounds with the ionized chemical elements of the gases that make up the plasma (nitrides, oxides). With change in the evaporation conditions the production of ultrafine powders and, during deposition, ultrathin films must be expected.

The investigations were conducted in the spectral range of 375–525 nm. The dynamics of the formation of the products from interaction of the atoms and ions of aluminum with the oxygen atom of the AlO radical was studied by

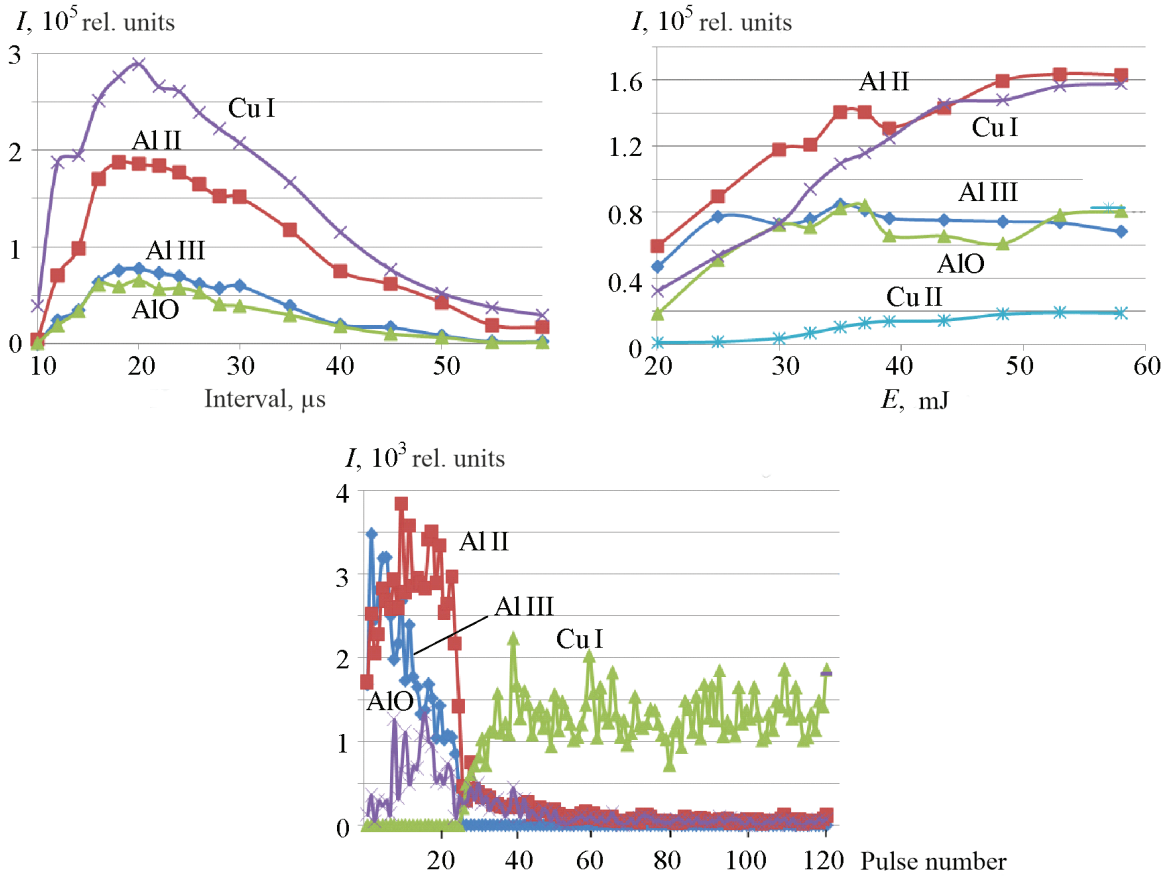

Fig. 1. Dependences of the intensity of the lines of the atoms and Al II (466.3 nm), Al III (452.92 nm), Cu II (493.165 nm), and Cu I (510.515 nm) ions and AlO band (484.22 nm) on the interval (a), the energy of the pulses (b), and the number of pulses (c).

means of the emission spectra of these molecules. The strongest electronic-vibration band of AlO in the emission spectra is the band at λ = 484.21 nm. The lines of Al II (466.3 nm), Al III (452.92 nm), Al III (361.92 nm), Cu II (493.165 nm), Al I (394.409 nm), Cu I (510.554 nm) and Cu I (515.324 nm) were used for analysis of the ionic and atomic composition and the parameters of the plasma.

The dependences of the intensities of the lines of the Al ions and Cu atoms and the bands of the AlO radicals on the interval between the pulses with 50 pulses per point and a pulse energy of 53 mJ are presented in Fig. 1a. The results from the investigations of the formation of the atoms, the Al and Cu ions, and the AlO radicals are shown in Fig. 1b. The experiments were carried out with a 10 μs interval between the laser pulses. The highest intensity of the atoms and ions and the molecular bands is observed in the range of 7–16 μs between the pulses. The intensity of the molecular bands at zero interval is close to zero. As seen from Fig. 1b, the formation rate of AlO radicals increases with increasing pulse energy up to 35–40 mJ and then decreases slightly, and at a pulse energy of ~50–60 mJ it returns to the values obtained at 35–40 mJ. The nonlinear dependence on the number of pulses is similar (Fig. 1c). The intensity of the molecular bands increases with increase in the number of pulses to 20–25 and then decreases substantially. The presence of such a sharp time threshold in the formation of the AlO radicals and Al and Cu nanoparticles indicates that the reason for the observed effects must be sought in the features of plasma formation inside the fairly deep microchannel that is formed.

In the double pulse method the heating and evaporation of the aerosols, nanoclusters, and fractals formed during exposure of the surface to the radiation of the first pulse are applied to the primary plasma formation processes by the second pulse. When a series of successive pulses is used a microchannel that acts as a micronozzle is formed. The latter makes it possible to reduce the size of the ablation products formed at the exit from the nozzle significantly as a result of rapid cooling, right down to nanometer size, in the expanding cloud. The formation of nanopowders of aluminum and copper

TABLE 1. Heat of Volatilization, Molar Volumes, and Layer Thicknesses Recorded for Al and Cu with Double Pulse

Parameter	Al	Cu	Ratio
Heat of volatilization, L_v, 10^6 J/cm^3	28.4	42.7	1.53
Molar volumes, V_{mol}, cm^3/M	9.997	7.124	1.40
Thickness at double pulse, h, μm	7.9	3.15	2.51
Average number of double pulses	24	86	3.5

oxides with particle sizes of 20–50 nm is achieved during interaction of the metal vapors with atmospheric oxygen under the conditions of turbulent agitation of the products. The intense cooling not only retards the growth of the particles but also increases the formation rate of the nuclei of the condensed phase.

To investigate the preparation of the nanopowder precursors we will examine the question of choosing the required number of pulses to obtain a stoichiometric ratio between the number of aluminum and copper atoms. The stoichiometric ratio of the number of copper and aluminum atoms in copper aluminate $CuAlO_2$ corresponds to their equality, i.e., their molar volumes in this case must be equal.

Figure 1c shows the results obtained during the successive action of a series of double pulses on a hybrid target consisting of plates of AD1 and M2 alloys stuck together at a pulse energy of 53 mJ and with an interval of 10 μs between the pulses. The number of pulses was 120, and the thickness of the plates was 0.23 mm. We will examine them in terms of a model of the surface evaporation of the metal on the assumption that nearly all the energy is used on the ablation of the substance. In such an approximation the thickness of the evaporated layer h (the amount of the substance) during the action of a pulse with given power density q depends on the duration of the action τ. For single-pulse radiation it can be estimated on the assumption that all the power delivered to the material goes to evaporation of the substance [18]:

$$h = V_v\tau = q\tau/L_v\,, \tag{1}$$

where V_v is the rate of vaporization of the substance (the rate of movement of the solid–gas boundary); L_v is the specific heat of vaporization of the substance (J/cm^3); q is the power density. In the intensive vaporization regime nearly all of the energy of the laser pulse is used on removal of the metal from the irradiated zone. The temperature of the surface amounts to $(2–3)T_{bp}$. As follows from (1), with a constant duration τ of action of the pulse on the surface the value of h increases in proportion to the increase of q. The ratio of the values of h for Cu and Al in this case is determined by the ratio of the L_I values for Cu and Al (Table 1).

The minimum power density of laser radiation q_{min} needed for the intensive volatilization of the metal can be calculated by means of the formula [19]:

$$q_{min} = 0.5kT\pi^{0.5}/A\alpha^{0.5}\tau^{0.5}\,, \tag{2}$$

where T_v is the volatilization temperature of the material; k is thermal conductivity; α is thermal diffusivity; τ is the duration of the action; A is the absorbing capacity of the material.

It should be noted that oxidation of the surface of the metals in the active zone of the laser pulse in air leads to increase of the absorbing ability of the surface. The rates of oxidation increase with temperature according the Arrhenius activation law. The characteristics of these processes are determined by the high rates of temperature variation realized during the action of the laser.

Approximate threshold values of the power density for the beginning of volatilization of aluminum and copper for the various values of A during the action of the pulse are presented in Table 2.

Under real conditions the volume of the evaporated material is less than the calculated value on account of the removal of heat from the irradiated surface well into the material due to thermal conductivity.

It is difficult to explain unambiguously the high rates of penetration when double pulses are used. Alongside the indicated mechanism of crater formation a cluster mechanism begins to play a role, i.e., due to the enormous thermal stresses and pressures in the irradiation zone a significant number of nanoparticles are taken out in the condensed phase.

As the radiation flux density of the laser increases the material heats up to higher temperatures. In a certain range of power density there is a distinct increase in the temperature growth rate for the series of metals. This means that the

TABLE 2. Approximate Threshold Power Densities (10^8 W/cm^2) for Volatilization of the Metals

Surface	*A*	Al	Cu
Pure	0.1	4.3	6.9
Oxidized	0.25	1.7	3.4
Oxidized	0.4	1.06	1.7

volatilization is no longer able to absorb all the energy of the laser radiation delivered to the metal. The surface of the irradiated material overheats, and a large part of the absorbed energy is converted into the internal energy of the expanding vapor. As a result the velocity of the evaporation front is no longer proportional to the density of the laser radiation flux. Comparison of the calculated and experimental threshold power densities shows that the experimental evaporation regime was chosen satisfactorily. The ablation rate and also the diameter of the microchannel are values that depend nonlinearly on the depth of the channel.

Results and Discussion. A pulse energy of 53 mJ and an interval of 10 μs between pulses were used in order to assess the possibility of the producing the nanopowders in practice. Irradiation was carried out with series of 110 double pulses on the target point. A total of 56 points with a step of 0.5 mm and 7 lines of 8 points per line were used. The size of the irradiation area on the target was 4 × 4 mm. The target was placed in a 40 × 20 × 30 mm glass cuvette covered with a lid.

A SEM image was used to analyze the products deposited on the surface of silicon plates mounted outside the laser flame zone (at the bottom and on one of the sides of the weighing bottle). The obtained SEM images of the synthesized nanoparticles and their agglomerates are shown in Fig. 2.

As a result of the action of laser radiation on the target in addition to cluster formation they are also assembled into mesoscopic disordered structures. It is seen that the structures have a branched structure and are organized hierarchically from finer fractal clusters. The effect of the gravitational mechanism of accumulation of the fractal aggregates on the substrate located at the bottom is more significant than for the purely diffusion mechanism on the side wall. The physics of this process and its control are of interest from the standpoint of the controlled production of such structures. The generally accepted model of the formation of branched fractal microscopic structures from the vapor–gas phase is the diffusion-restricted aggregation model. In the discharge plasma the aggregation is preceded by two processes: the formation of molecular associates and the condensation of the vapor. The condensation centers, around which liquid droplets are formed, are predominantly ions. During collision with each other the associates grow and become denser, and this also leads to formation of the nuclei of the liquid phase. The drop (compact cluster) model is regarded as the limiting case of an object with the maximum number of bonds in the cluster. The other limiting case is the model of an associate with the minimum number of bonds where the atom only interacts with a pair of nearest neighbors. Such an object is called gas-like since it cannot be characterized by a specific volume and density. The question as to which model is more suitable for description of the properties of clusters at high temperatures in a dense vapor phase is of interest for both fundamental science (a nonideal plasma and nucleation theory) and the modern technology for the creation of new unusual structures. The size of the primary particles is 30–45 nm, and the particles are assembled into agglomerates and have crystalline structure and spherical form.

The spherical form of the nanoparticles produced under extreme conditions indicates that during cooling the particles spend some time in the liquid state and are subject to enormous pressure on account of Laplace compression. In such a state the pores, voids, etc. are packed onto the surface of the particle. The only type of nanoparticle defects formed under extreme conditions is the displacement of atoms in relation to the equilibrium position. As noted in [20–22], the most important problem directly associated with the dimensional dependence of the surface tension is the thermodynamic stability of the nanoparticles.

By laser vaporization of the substances, including the heat-resistant ones, it is possible to achieve high efficiency in the generation of compact clusters and their aggregates. Initially molecular associates (dimers, trimers, etc.), the concentration of which can amount to 0.1 in relation to the monomers, are formed in the saturated vapor. After 10^{-4} s compact clusters containing 10^3–10^4 atoms appear as a result of condensation of the vapor and coagulation of the nuclei of the liquid phase in the cooled layers of the vapor–gas stream [23]. The effectiveness of cluster formation increases in the atmosphere of a buffer gas, which brings with it an excess of the energy released during condensation. By aggregation the compact particles with a characteristic size of ~10 nm form fractal clusters (aggregates) with a size of ~1 μm. The latter

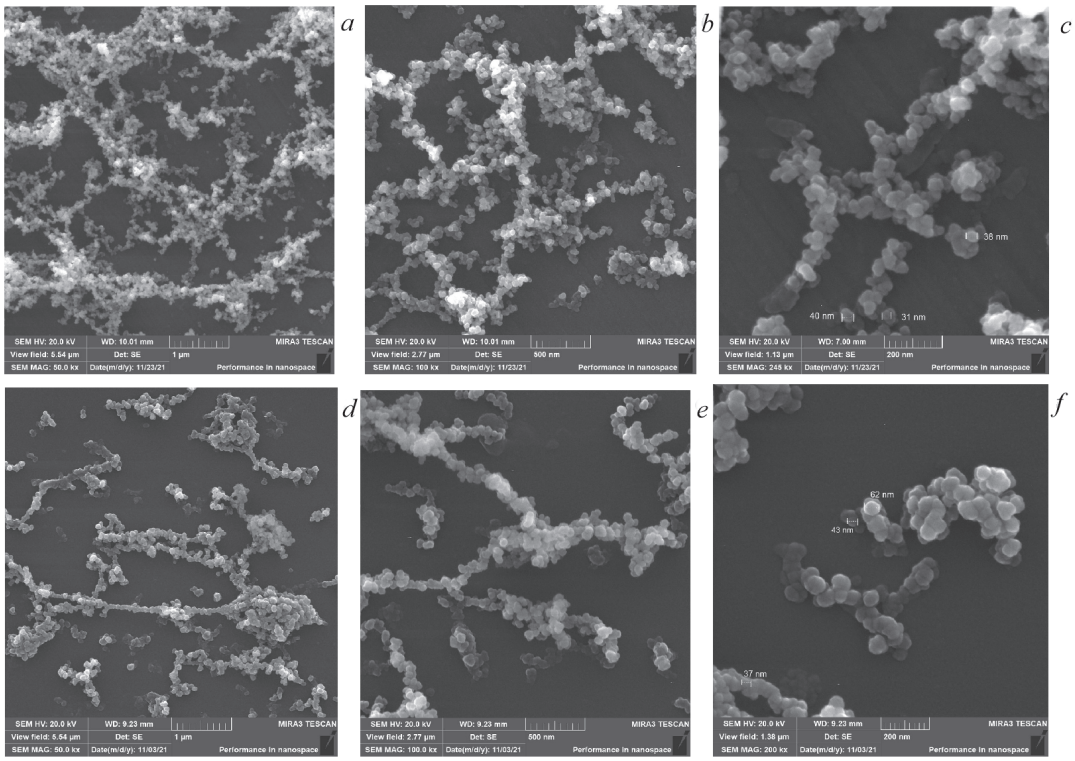

Fig. 2. The SEM images of the nanoparticles and the agglomerates on the bottom (a–c) and on the side (d–f).

are observed ~10^{-2} s after the action of a millisecond laser pulse with a flux density of 10^6–10^7 W/cm^2 [23]. In an external electric field the fractal aggregates assemble into filamentary microstructures. According to [23] the fractal filaments appear 10^2–10^3 s after the action of the laser pulse. During longer laser exposure and, accordingly, with a higher density of the finely dispersed fraction in the volume of the flame a mechanism of microstructure formation that differs from aggregation is realized. Thus, with a 10-fold increase in the duration of the laser pulse macrostructures appear after ~10^{-2} s even in the absence of an external field. The mechanism of macrostructure formation in this case is presumably triggered by percolation transition in the cluster of microfractals.

The fractal structures that form in the vapor-gas phase close to the target surface during the action of the laser pulse are percolation clusters, which can be formed particularly from the compact microclusters that appear during condensation. For rapid (nonaggregation) formation of fractal macroformations [23] from the percolation structures it is necessary that the latter do not collapse during expansion of the plasma flame. This is possible in the presence of attractive forces between compact microclusters located at the nodes of the percolation cluster.

When deposited on a substrate the clusters form fractal layers. The distribution of the substance in them depends on the characteristics of the clusters (thermal energy, size, charge, dipole moment, dimensionality, etc.), their numerical density, and the characteristics of the surface. A model experiment that takes account of the deposition of the clusters on the substrate, their diffusion over the surface, and their aggregation into substantial structures was presented in [24]. It was shown that the morphology of the fractal layer depends on the ratio between the dimensions of the system L and the characteristic scales (the diffusion length L_1 and the average distance between the growing structures L_2) and can correspond to various models of the growth of the structures. Thus, the cluster morphology that arises in the diffusion-limited aggregation process is realized in the case of low particle fluxes and small system sizes compared with the diffusion length ($L < L_1$). The cluster–cluster aggregation model is realized with small fluxes and with a small diffusion length ($L_1 < L < L_2$). The percolation cluster model corresponds to the structures formed with high fluxes and large system dimensions. The presence of a dipole moment in the deposited particles and long-range interaction between them leads at sufficiently low temperatures to the appearance of ordered structures (chains) [23].

TABLE 3. The Melting Points (K) of the Metal Oxide Nanoparticles

Compound	Bulk	*R*, nm		
		10	25	50
Al_2O_3	2317	695	927	1993
CuO	1720	360	1376	1548

The products of chemical reaction, the formation of particles with various compositions, the complex morphology of the particles, and the unavoidability of diffusion of the components in the condensed phase have a complicating effect on the type of distribution of the particles. With the simultaneous realization of two conditions — a fairly high temperature (usually above $2/3T_s$, where T_s is the softening temperature of the nanoparticles) and strong interaction between the nanoparticles — coalescence occurs. In this case, during the time of the interaction between the nanoparticles the particles merge, and their original shape is lost, and a single particle with a more equilibrium configuration is formed. At even higher temperatures coalescence of the solid nanoparticles occurs so rapidly that it resembles the merging of two liquid drops and is called liquid-like coalescence. If the nanoparticles have nonequilibrium shape and a very rough surface then as a result of the diffusion processes each nanoparticle contracts under the influence of surface tension forces and is rounded off, leading to a more equilibrium shape. This process is called autocoalescence. Here it is necessary to take account of the fact that the melting point of the nanoparticles of aluminum and copper oxides is lower than for the bulk material. Table 3 shows the melting points of the bulk samples of aluminum and copper oxides and also of the samples with sizes r = 10, 25, and 50 nm [25].

The particles that settle on the walls often stick to each other, forming tangled chains. It is very difficult and sometimes almost impossible to separate the sticking chains. The surface of the particles is so active and clean that the small particles can stick to each other at temperatures below the melting point of the original substance. This indicates the existence of a low temperature limit for production of the smallest particles of the material. Thus, the actual finest particle that can be used in practise must always be coated with a protective layer and/or be kept at the lowest possible temperature.

It should be noted that obtaining the thermodynamic parameters for the agglomerates of aluminum oxide is complicated by the fact that they do not exist in the gas phase, and according to the basic models of homogeneous condensation from supersaturated vapors it is necessary to know the state parameters both for the condensed and for the gas phase. The clusters of aluminum oxide are formed as a result of the adhesion reactions of its various suboxides (AlO, AlO_2), and for accurate determination of the thermodynamic parameters of the aluminum oxide cluster it is necessary to know the substances on account of which it is formed and also the composition of the saturated mixture in the equilibrium and nonequilibrium states. Starting from the differences in the partial pressures in the equilibrium and nonequilibrium states it can be concluded that the main flow of the mass for the formation of the Al_2O_3 clusters and also their growth occur as a result of reactions that make the most noticeable contribution: $2AlO + O \leftrightarrow Al_2O_3$ and $Al_2O + O_2 \leftrightarrow Al_2O_3$.

The difference in the partial pressures of the remaining components, such as AlO_2, Al_2O_3, and others, is insignificant, and there is consequently no noticeable increase in the weight of the full oxide as a result of their fusion.

Copper aluminate can be formed in the reaction of both CuO and Cu_2O with Al_2O_3: $2CuO + Al_2O_3 \rightarrow 2CuAlO_2 + 1/2O_2$, $Cu_2O + Al_2O_3 \rightarrow 2CuAlO_2$.

A separate important question is the resistance of $CuAlO_2$ as a compound of monovalent copper to oxidation. According to the phase diagram it can be expected that this compound is oxidized in air at temperatures of 300–1000°C. This assumption was verified in [12], and it was found that no mass gain was observed; the $CuAlO_2$ compound is therefore fairly resistant to oxidation in air under the experimental conditions at 20–1000°C, which was confirmed by x-ray diffraction (extraneous phases did not appear). This is explained by the kinetic stability of the compound. The abrupt decrease of the weight by 0.3% at 1015°C is due to fusion-related dissociation of the impurity present in the sample $CuO \rightarrow Cu_2O + O_2$.

Let us examine the qualitative results. Plasma formation in air becomes much more complicated due to an aftereffect that is almost inevitable with the formation of deep holes by the double pulses as a result of the accumulation of ablated microparticles and clusters in the atmosphere of the cavities. Here the impact of a pulse following after a short time interval leads to a low-threshold optical breakdown of the air saturated with metal microparticles and to the appearance of two plasma formations simultaneously separated in space. One of them is a conventional laser plasma flame on the ablated

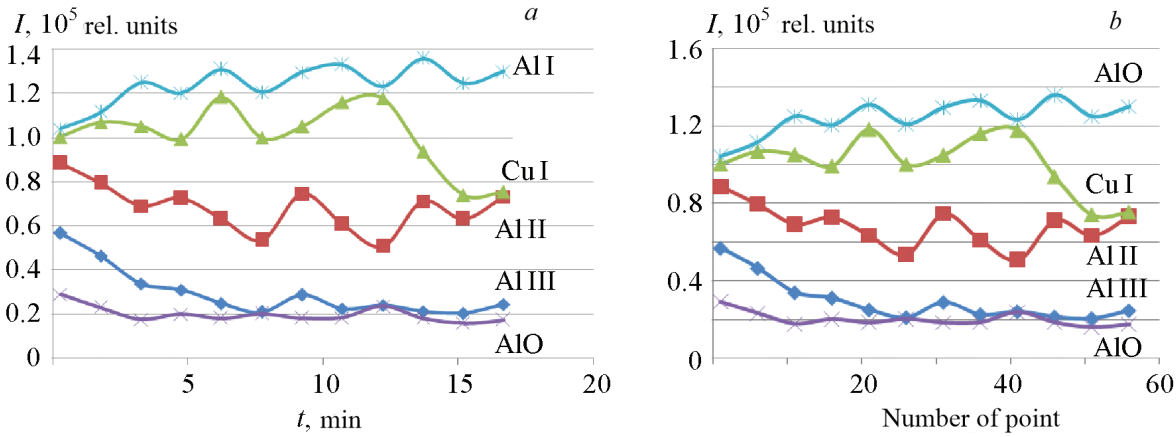

Fig. 3. Dependence of the intensity of the lines on time (a) and on the number of the point (b).

surface and at the bottom of the hole, while the other is a plasma–dust cloud that also appears on the axis of the laser beam but is separated by a certain distance from the surface. In this case the appearance of a plasma–dust region at a certain distance from the surface leads, on the one hand, to additional screening and more importantly, on the other, to the creation of a high-temperature high-pressure plasma cloud that extends predominantly in the direction of the hole.

The development of the processes with time in air and in the laser flame is shown in Fig. 3. The average time taken for the ablation process at a single point of the target and the transition to the next point amounts to ~17.86 s. Strong dependence of the intensity of all the lines on time is observed. The intensity of the lines of the aluminum ion decreases by several times even with a small number of broken points; the same is observed for the AlO band. Here the intensity of the atomic line of Al and the line of Cu increases by ~20%. In the following period the intensity of the atomic and ionic lines of Al remains constant. The intensity of the Cu line after the 40th point decreases by almost a factor of two. We will analyze the results in the light of the mechanism of the previously published mechanism of rapid formation of fractal clusters from percolation structures in the laser flame [23].

Laser volatilization of the condensed media produces numerous types of clusters and cluster structures. Microclusters are formed effectively during the action of short laser pulses [26]. After the action of a double laser pulse on the target a large number of compact microparticles are formed in the expanding laser flame, depending on the experimental conditions, and fractal microclusters [27], giant fractal clusters [28], and fractal filaments [29] are formed from them. In [30] the thermophysical parameters of a low-temperature plasma during the evaporation of metals by laser radiation of moderate intensity were analyzed, and the processes leading to the formation of compact microclusters in the vapors of an expanding flame with decrease of temperature were examined. It was found that fractal structures including gigantic fractal clusters are formed directly after the end of the laser pulse in the course of <0.1 s. It is assumed that the rapid formation of the fractal clusters is closely related to the occurrence of percolation in the laser flame [31].

In [31] it was shown that after the end of the heating laser pulse linear and branched aggregates, uniformly distributed over the entire closed volume, are formed as a result of cluster–cluster aggregation. The time for the establishment of a uniform distribution of the scattering particles in the chamber is ~5 min, and the particle density is $\sim 10^6$–10^7 cm^{-3}. The initial clusters may be formed as a result of aggregation of the compact microclusters that condense in the expanding plasma or of evolution (destruction) of the percolation structure that exists at the moment of the action of the laser pulse.

The fractal structures that are formed in the vapor–gas phase on the surface of the target during the action of the pulse of laser radiation are percolation clusters that can be formed, in particular, from the compact microclusters that appear during condensation. For rapid (nonaggregation) formation of fractal macroformations from the percolation structures it is essential that the latter are not destroyed during expansion of the laser flame. This is possible in the presence of forces of attraction between the compact microclusters at the nodes of the percolation cluster.

The observed nonlinear dependence of the intensities of the Cu lines, particularly for the last ablation points, can be explained quantitatively in the following way. Under repeated pulsed high-intensity action of the laser at one point of the target a mass of the target material is removed as a result of laser ablation, and a channel is formed. During the formation of

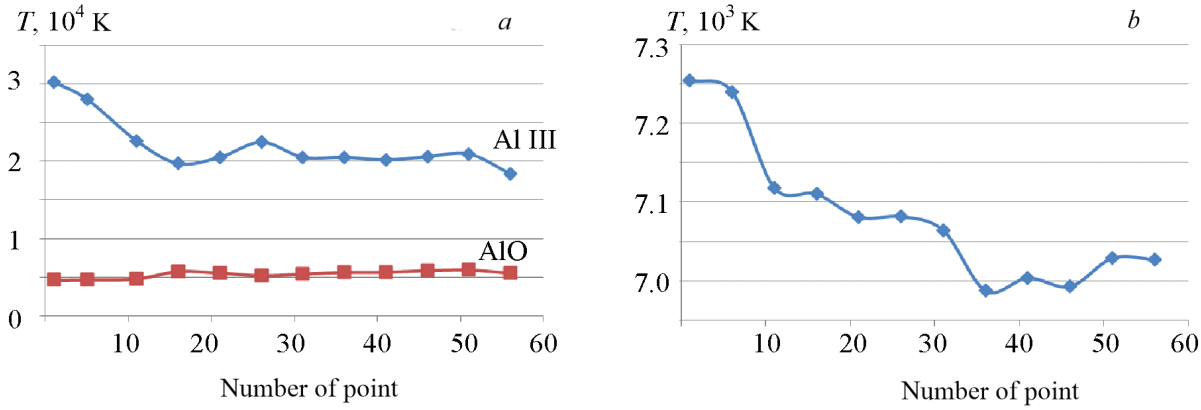

Fig. 4. Dependence of the temperature in the regions of formation of Al III ions and aluminum suboxides AlO (a) and the surface plasma over the surface of the copper on the number of the point (time) (b).

the channel the physical picture of the accompanying processes is greatly complicated compared with the situation where the laser radiation falls on the smooth surface of the target. Concentration of the laser radiation in the channel leads to increased absorption of the energy of the pulse and, accordingly, to increase of the plasma temperature and to increase of the effectiveness of formation of the ions. Here after the action of the first pulse a suspension ("cloud") containing nano- and microparticles of the target (clusters) can form inside the channel. Interaction of the laser radiation of the second pulse with such a cloud in the plasma formation regime leads to self-action, partial screening, and problems in delivery of the radiation energy to the bottom of the channel and, consequently, to change in the shape of the channel [32–34].

With increase in the depth of the crater formed during repetitively pulsed laser action on the target the conical microchannel that forms can serve as an analog of a nozzle passing through which the substance of the target form clusters more effectively. The concentration of the clusters and their distribution behind the nozzle exit are determined by the geometry of the nozzle. During expansion of the gas through the nozzle not all of the atoms, ions, or molecules of the gas but only a certain percentage of them form clusters. It can be argued that screening during the action of air on the particles only appears when the channel reaches aspect ratios A (the ratio of the depth to the diameter of the channel) greater than unity, which is due to removal of the particles from the crater at lower values of A as a result of convective air flows.

For typical intensities of laser pulses $q \approx 5.10^6$ W/cm^2 the spread rate and temperature of the plasma in the second phase amount to $3 \cdot 10^6$ cm/s and $3 \cdot 10^5$ K [35, 36]. With allowance for the spread rate and the average duration of the laser pulse (15 ns) toward the end of this phase we obtain the length of the plasma flame with unidimensional extension of ~0.45 mm, which is comparable with the length of channel. As a result during the action of the second laser pulse the plasma reaches the surface of the sample, and its further spread takes a form approximating to hemispherical. The expansion practically stops when its internal region reaches atmospheric pressure. A greatly restricted and relatively long-lived region of hot gas is formed close to the irradiated surface.

The degree of ionization of the laser plasma formed after the action of the second pulse on the condensation products is higher that in the plasma close to the surface. This is demonstrated by an increase of practically an order of magnitude in the intensity of lines of the Al ion with increase of the number of pulses. The temperature of the laser plasma is of course much higher than that of the plasma close to the surface.

The formation of the aluminum oxides is restricted by a strictly defined range of thermodynamic parameters: pressure, temperature, concentration of dissociation products in the gas phase, and the presence or absence of the condensed phase. Almost complete dissociation of the aluminum oxide phase Al_2O_3 to the oxides AlO and Al_2O is ensured temperatures of >4800 K. At temperatures below 3000 K the degree of dissociation of Al_2O_3 is <1 %. The suboxides also decompose into the simple ions at high temperature. Thus, for AlO the boiling point is 2253 K while the decomposition temperature is 4400 K [35, 36], i.e., the optimum for the formation of the AlO suboxides is a laser plasma in the region of ~4400–5500 K and, after further cooling and turbulent mixing of the vapors, suboxides with air at the exit of Al_2O_3 nanodroplets from the micronozzle. Figure 4a shows the results from determination of the temperature in the region of the formation of AlO by means of the equation in [34]. It is seen that the most favorable conditions for the formation of AlO are

those for the first 10 points. This agrees well with the results presented in Fig. 3 — a decrease of ~1.5 times in the intensity of the AlO band.

A similar decrease of intensity was observed for the ion lines of Al III. The temperature in the region of the formation of Al III is determined by the Ornstein method based on the ratio of the intensities of the spectral lines of Al III (452.9 nm, E_{k1} = 20.55 eV, and 360.16 nm, E_{k2} = 17.81 eV). The dependence of the average temperature of a laser plasma in the region of Al III on the number of the point (time) is presented in Fig. 4a. A sharp drop of temperature from 30,000 to 20,000 K is observed. The temperature of the surface plasma of copper, formed in the microchannel after passing through the aluminum layer, calculated by the Ornstein method in relation to the lines of Cu 510.515 to 515.324 nm, is presented in Fig. 4b. It is seen that as the number of large fractals (36–40 points) in the air accumulates and the energy losses of the pulse increase due to scattering of the energy and absorption the temperature drops by almost 250^{o}C while the line intensity decreases by almost a factor of two.

Conclusions. The use of an interval of 7–16 μs between the pulses ensures an increase of several orders of magnitude in the concentration of Al and Cu and of the products of their interaction with atmospheric oxygen compared with the zero interval. The largest increase in the concentration of nanopowders containing aluminum and copper oxides is obtained by two-pulse ablation of the target by double pulses with an interval of 10 μs between the pulses and an energy of more than 45–50 mJ. The largest contribution to change in the intensity of the spectral lines of Al and Cu atoms and ions and the AlO molecular bands is obtained by interaction of the second pulse with the condensation products formed in the channel after the first pulse. With increase in the number of fractal aggregates in air the intensity of the molecular bands and lines of Al III decreases by ~1.5 times while that of copper decreases by almost two times. This is due to active interaction of the long-lived large fractals that accumulate in the air with the incident radiation, i.e., by scattering and absorption. The size of the primary particles, determined by high-resolution electron microscopy, ranged from 30 to 45 nm. The particles are assembled into agglomerates and have a crystalline structure and spherical shape.

The positive results of the experiments as a whole should be regarded as the basis for further work on improving the production of precursor nanopowders for the manufacture of nanoceramics of the $CuAlO_2$ type. There is also the possibility of significantly expanding the range of mixed $CuAlO_2$ nanopowders doped with divalent metal cations such as Ca^{2+} and Mg^{2+}, in which the hole conductivity of the material is much higher.

REFERENCES

1. R. A. Andrievskii and A. V. Ragulya, *Nanostructural Materials* [in Russian], Textbook, Akademiya, Moscow (2005).
2. A. I. Gusev, *Nanomaterials, Nanostructures, Nanotechnologies* [in Russian], Fizmatlit, Moscow (2007).
3. Yu. I. Petrov, *Physics of Small Particles* [in Russian], Nauka, Moscow (1982).
4. S. P. Bardakhanov, A. I. Korchagin, and N. K. Kuksanov, *Dokl. Akad. Nauk*, **409**, No. 3, 320–323 (2006).
5. V. V. Osipov, O. M. Samatov, M. G. Ivanov, V. V. Platanov, and A. M. Murzakaev, *ZhTF*, **74**, No. 3, 72–77 (2004).
6. M. G. Ivanov, Yu. A Kotov, V. P. Komarov, O. M. Samatov, and A. V. Sukhov, *Fotonika*, No. 3, 18–20 (2009).
7. S. V. Zabotnov, A. A. Ezhov, L. A. Golovan′, M. A. Lastovnika, V. I. Panov, V. Yu. Timoshenko, and P. K. Kashkarov, *FTP*, **41**, No. 8, 1017–1020 (2007).
8. B. I. Stepanov, *Dokl. AN BSSR*, **V**, No. 12, 541–544 (1961).
9. B. I. Stepanov and V. P. Gribkovskii, *Izv. AN SSSR*, **XXIV**, No. 5, 534–538 (1960).
10. H. Kawazoe, M. Yasukawa, H. Hyodo, M. Kurita, H. Yanagi, and H. Hosono, *Nature*, **389**, 939–942 (1997).
11. N. Benreguia, A. Barnabe, and M. Trar, *J. Solgel Sci. Technol.*, **75**, No. 3, 670–679 (2015).
12. V. A. Kul′bachinskii, V. G. Kytin, D. Yu. Kondrat′eva, A. N. Grigor′ev, A. A. Kamenov, V. A. Amelichev, and I. E. Korsakov, *Mezhdunar. Zh. Prikl. Fundam. Issled.*, Nos. 1–2, 223–227 (2017).
13. J. Tate, H. L Ju, J. C. Moon, A. Zakutayev, A. P. Richard, J. Russell, and D. H. McIntyre, *Phys. Rev. B*, **80**, No. 16, Article ID 65206 (2009).
14. O. J. Dur′a, R. Boada, A. Rivera-Calzada, C. Le′on, E. Bauer, M. A. L′opez de la Torre, and J. Chaboy, *Phys. Rev. B*, **83**, Article ID 045202 (2011).
15. R. D. Shannox, D. B. Rogers, and C. T. Prewitt, *Inorg. Chem.*, **10**, 713–718 (1971).
16. B. U. Kohler and M. Jansen, *Z. Anorg. Allg. Chem. B*, **543**, 73–80 (1986).
17. V. K. Goncharov, V. I. Karaban′, and V. A. Obromenkii, *Kvantovaya Élektron.*, **15**, 1235–1240 (1986).
18. A. P. Menushenkov, V. N. Nevolin, and V. N. Petrovskii, *Physical Principles of Laser Technology* [in Russian], Textbook, MIFI, Moscow (2010).

19. V. P. Veiko and E. A. Shakhno, *Laser Technologies in Tasks and Examples* [in Russian], Textbook, St. Petersburg State Institute of Information Technology, Mechanics and Optics, St. Petersburg (2014).
20. V. M. Samsonov and N. Yu. Sdobnyakov, *Poverkhnost'. Rentgenovskie, Sinkhrotronnye Neitronnye Issled.*, No. 2, 73–78 (2004).
21. N. Yu. Sdobnyakov, B. M. Samsonov, A. N. Bazulev, D. A. Novozhilova, and D. N. Sokolov, *Vestn. Novgorod. Gos. Univ. imeni Yaroslava Mudrogo. Ser. Tekh. Nauki*, No. 5, 43–48 (2017).
22. N. A. Romanov, A. V. Nomaev, and S. V. Kalashnikov, *Vestn. Buryatsk. Gos. Univ.*, No. 3, 93–99 (2013).
23. N. E. Kask, S. V. Michurin, and G. M. Fedorov, *Kvantovaya Élektron*., **33**, No. 1, 57–68 (2003).
24. P. Jensen, A.-L. Barabási, H. Larralde, Sh. Havlin, and H. E. Stanley, *Phys. Rev. B*, **50**, 15316–15330 (1994).
25. V. M. Yurov, V. Ch. Laurinas, and S. A. Guchenko, *Mezhdunar. Zh. Prikl. Fundam. Issled.*, No. 1, 38–42 (2019).
26. Y. J. Twi, C. W. S. Conover, Y. A. Yang, and L. A. Bloomfield, *Phys. Rev. B*, **42**, 5306–5316 (1990).
27. A. A. Lushnikov, A. V. Pakhomov, and G. A. Chernyaev, *Dokl. Akad. Nauk SSSR,* **292**, 86–88 (1987).
28. N. E. Kask and G. M. Fedorov, *Kvantovaya Élektron*., **20**, No. 6, 527–528 (1993).
29. A. A. Lushnikov, A. E. Negin, A. V. Pakhomov, and B. M. Smirnov, *Usp. Fiz. Nauk*, **161**, No. 2, 113–123 (1991).
30. B. M. Smirnov, *Usp. Fiz. Nauk*, **164**, No. 7, 665–703 (1994).
31. N. E. Kask, *Pis'ma ZhÉTF,* **60**, No. 3, 204–208 (1994).
32. Kh. Bazzal, N. A. Alekseenko, E. S. Voropay, M. N. Kovalenko, N. H. Trinh, and A. P. Zazhogin, *J. Appl. Spectrosc.*, **88**, No. 1, 85–91 (2021).
33. Kh. Bazzal, E. S. Voropai, A. P. Zazhogin, and M. P. Patovich, *Physicochemical Aspects of Studying Clasters, Nanostructures, and Nanomaterials*, Interinstitutional Collection of Sci. Papers, No. 11, Tver, 48–56 (2019).
34. Kh. Bazzal, N. A. Alekseenko, E. S. Voropay, M. N. Kovalenko, M. P. Patapovich, and A. P. Zazhogin, *J. Appl. Spectrosc.*, **88**, No. 2, 274–282 (2021).
35. S. M. Garnov, V. I. Klimentov, T. V. Konov, S. V. Kononenko, and F. Dausinger, *Kvantovaya Élektron*., **25**, No. 1, 45–48 (1998).
36. G. E. Belyaev, A. M. Velichko, V. P. Dubenkov, M. N. Larichev, A. I. Nikitin, A. E. Sheindlin, E. I. Shkolnikov, and I. V. Yanilkin, *TVT*, **50**, No. 6, 804–809 (2012).